

# Convolutional Neural Network-Based Low Light Image Enhancement Method

M.X. Li<sup>1</sup>, C.J. Xu<sup>2</sup>

<sup>1</sup> Institute of Big Data and Artificial Intelligence, Zhengzhou University of Science and Technology, Zhengzhou, 450064, China;

<sup>2</sup> Informatization Center, Zhengzhou Information Engineering Vocational College, Zhengzhou, 451000, China

## Abstract

With advances in science and technology, remote sensing images are vital for vegetation monitoring. The use of remote sensing allows for the collection of widespread, multi-temporal data on vegetation, leading to a better comprehension and management of natural resources. In this study, a new remote sensing image recognition model is proposed by combining the filtering algorithm to reconstruct the time series curve, fusing the quadratic difference method and decision tree, and introducing the morphological similarity distance method. The results of the experiment indicate that the normalized vegetation index in towns was consistently higher than the index in bodies of water throughout the year. The normalized index for water was generally close to or below 0. Additionally, the normalized index for forests surpassed that of both water and towns. Although the waveforms for all three were similar, the differences were significant. Notably, the forest normalized index curves had a single peak with a noteworthy duration. The study found that the mapping accuracy for fall plants was highest in 2013 (97.37%) and lowest in 2014 (80.00%). Similarly, for spring vegetation, the mapping accuracy was greatest in 2017 (97.96%) and lowest in 2014, but still favorable at 90.00%. These results highlight the high advantages of the remote sensing identification method proposed by the study for vegetation identification, which is crucial for natural resource management and environmental protection.

**Keywords:** filtering algorithms; time series curves; remote sensing imagery; normalized vegetation indices.

**Citation:** Li MX, Xu CJ. Convolutional Neural Network-Based Low Light Image Enhancement Method. *Computer Optics* 2025; 49 (2): 334-343. DOI: 10.18287/2412-6179-CO-1499.

## Introduction

Remote sensing imagery plays a crucial role in monitoring vegetation. This technique, which relies on a combination of spectra, texture, machine learning, and time series, offers a comprehensive and accurate method of obtaining valuable vegetation data. As a result, it provides important decision-making support for natural resource management and environmental protection. RS technology is a significant component of remote sensing imagery and plays a crucial role in advancing modern science and society while gathering vast amounts of data on the Earth's surface [1]. Nonetheless, the quality of RS data is often hindered by considerable noise and other factors, leading to certain issues with data quality [2]. To enhance the quality and usability of data, filtering algorithms (FAs) are extensively employed in RS data processing to enhance the completeness and accuracy of vegetation monitoring methods. The study proposes a new artificial intelligence RSI recognition model that utilizes FAs reconstruction time series curves (TSCs). The model combines the quadratic difference method and decision tree to investigate vegetation changes and recurrence indices. The aim is to improve the ability to recognize the vegetation situation and enhance the accuracy of RS recognition. The study is organized as follows: the scientific background, significance, and prospects for RSI recognition are described in the first section. The second part concentrates on the algorithm flow created in this re-

search, which is grounded in FAs reconstruction TSC and represents the focal point and the innovation of the study. Building on the design of the second portion and the analysis of the experimental data results, the third section gives a detailed overview of the algorithm's experimental validation. Lastly, the fourth section concludes on the experimental results, outlines the limitations of this design, and presents future development directions. The final section summarizes the experimental results and outlines limitations in the design along with directions towards future development.

## 1. Related works

The time series method has been widely utilized in the RSI technique for vegetation recognition to classify plant species due to plant growth's periodicity. In order to improve the recognition resolution and technical improvement of vegetation geological features, many researchers have conducted research on Remote Sensing Information (RSI) technology. Sun C and the team proposed a salt marsh vegetation classification method, which uses time series cloud cover to construct pixel difference time series (PDTS) with different observation distributions for each pixel; Using phenological parameters derived from Sentinel-2PDTS, using a tidal filter determined by the threshold and frequency of the Modified Normalized Difference Water Index (MNDWI) to exclude tidal related observations from PDTS; Phenolic parameters are used as classification features, and with the assistance of sample

data, the random forest algorithm is applied to plant species classification. According to experiments, there was a 5.1% improvement in the total accuracy of PDTS-based plant species classification, with an average accuracy of 81.5% [3]. The optimal slope time division filtering (BSTS) approach was introduced by Bao R et al. to increase the estimation accuracy of red pine above ground biomass (AGB). The time series segments were split to create the reconstructed time series, and multiple linear regression and random forest regression (RFR) techniques were used to estimate the AGB of thick pine [4]. Liu and other scholars characterized EFT at county scale based on Subtractive fuzzy clustering mean (SUBFCM) and Sentinel-2-time series data. Ecosystem function indicators were selected to characterize regional EFT diversity patterns. The results showed that the SUBFCM algorithm can automatically divide the EFT with faster convergence and reduced subjectivity. The distribution pattern of ecosystem functional diversity and the internal structure of carbon balance were both reflected in the Sentinel-2 image [5]. Lian X and his team proposed a monitoring method for coal mining subsidence in mountainous areas based on time series unmanned aerial vehicle photogrammetry technology. The algorithm was used to filter the overall point cloud data of the study area, resulting in a Digital Elevation Model (DEM). The dynamic subsidence basin on the surface was determined through two stages of DEM subtraction. The greatest accuracy of subsidence monitoring was 98%, and the average root mean square error was 165 mm, according to the results [6]. Fan et al. proposed an iterative algorithm for dynamic load recognition based on Newmark-beta, which added a kind of self FAs to the load recognition algorithm. The results showed that the algorithm had high recognition accuracy and computational efficiency [7].

The problem of noisy images arises during RS recognition, Yang et al. proposed a new low-pass FAs to remove noise and solve these problems. Based on the summation properties of signal and noise in GRACE data, an alternative evaluation method was investigated and applied to denoise the dEWH dataset. The results show that the algorithm has no data ambiguity, eliminates the maximum noise in residual analysis evaluation, and preserves the maximum signal evaluated by the large root mean square (RMS) value [8]. Rayegani develops an integrated approach to identify dust storm source trends from RS data and generates wind erosion sensitivity maps through multi-criteria assessment after spectral vegetation index and classification preprocessing of Landsat data. The results showed that time series analysis of Remote Sensing (RS) data demonstrated high capability [9]. To precisely and efficiently support production scheduling and deployment in mining areas, Wang and Tian looked into the extraction of feature information in the area. Analysis was done on the hyperspectral RS imaging technology's detecting capacity. Each group of mapping results is divided using the spectral matching approach,

and the extraction of ground feature information – which is crucial for safe production in mining areas – is carried out by the deep learning algorithm. The research revealed the development of the hyperspectral RS rock and mineral feature information extraction module, which first made it possible to acquire typical mineral information quantitatively and accurately [10].

In summary, researchers have studied data recognition and algorithm classification for RSI recognition, but the application of FAs for improved recognition is insufficient. Thus, this study proposes a novel artificial intelligence RSI recognition method based on filtering arithmetic to reconstruct the TSC. This method is used for recognizing the geographic features of vegetation classes and providing a technical basis for environmental geology RS surveys.

## 2. FA-based time series reconstruction in RSI identification

Remote sensing technology plays an important role in modern society, providing a large amount of remote sensing data by obtaining and analyzing distant ground information. There are problems such as noise in RS image processing, which seriously affects the effect of vegetation RS recognition and classification, so the study combines FAs to process it to improve RS recognition accuracy and ability enhancement.

### 2.1. Reconfiguration study of NDVITSC based on FA

The normalized digital vegetation index (NDVI), the best indicator of the condition of vegetation growth and vegetation cover to assess the vegetation cover, is used in the study to identify the geographic characteristics of vegetation classes [11]. The calculation equation is shown in Equation (1).

$$NDVI = \frac{NIR - Red}{NIR + Red}. \quad (1)$$

The reflectance values in the red band are represented by the letter  $Red$  in equation (1), and the reflectance values in the near-infrared band by the letter  $NIR$ . In order to reduce the data storage capacity as well as the arithmetic speed of the data processing matter, this study multiplied all the NDVI values by 10000. In the process of RS identification, the noise problem arises, so the corresponding FAs were introduced, including the hyperlink induced topic search (HANTIS) algorithm [12]. HANTIS filtering for reconstructing the time series of RS data is analyzed by the superposition of the function and the signal period function as in Equation (2).

$$\begin{cases} \hat{y}(t_j) = a_0 + \sum_{i=1}^{nf} [a_i \cos(2\pi f_i t_j) + b_i \sin(2\pi f_i t_j)], \\ y(t_j) = \hat{y}(t_j) + \varepsilon(t_j). \end{cases} \quad (2)$$

In Equation (2),  $\hat{y}$ ,  $y$  and  $\varepsilon$  are the original, reconstructed and error sequences, respectively.  $t_j$  is the time of obtaining  $y$ ,  $j = 1, 2, \dots, N$ , where  $N$  is the maximum num-

ber of samples in the time series. The flowchart of the implementation of HANTIS is shown in Fig. 1.

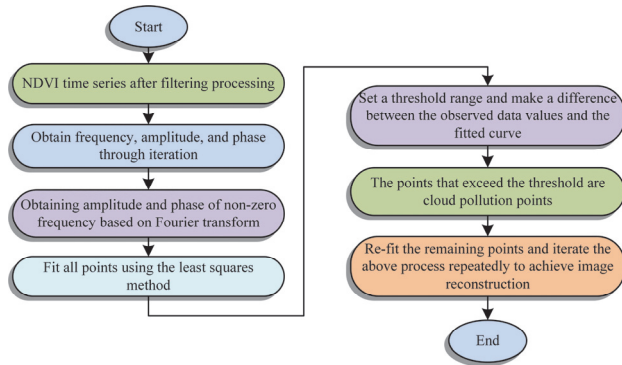


Fig. 1. Implementation of HANTIS

The S-GFA proposed by Savitzky et al. is a FAs based on the least squares product fitting of local polynomials. The lack of strict requirements on the type of NDVI data or sensors is the most important feature of the S-G filter, so that the noise is filtered out while ensuring that the shape and width of the signal remain unchanged [13–14]. The least squares method is used to fit a multi-step polynomial applied to the number of points around a selected point, and the average value of the point is calculated by the polynomial, and the original sequence is processed as a weighted average. The specific expression is shown in Equation (3).

$$Y'_j = \sum_{i=-n}^{i=n} \frac{C_i Y_{j+1}}{N} \quad (3)$$

In Equation (3),  $N$  represents the window size  $L=(2N+1)$ ,  $Y'$  value represents the predicted value, i.e., the original data,  $C_j$  represents the value of the weighted number of the first  $i$  number,  $n$  represents the range of the moving window, the size of the  $n$  value represents the number of peaks and valleys that are smoothed, the larger the value, the smoother the result is,  $Y_{j+1}$  represents the  $(j+1)$ -th data of the data in the time series, and  $j$  is the  $j$ -th data in the time series. One aspect influencing the effect of RS is noise; therefore, the study integrates the widely-used FA--EMD approach to improve the denoising effect on the original data. Empirical Mode Decomposition (EMD) filtering algorithm is an adaptive data processing method suitable for smooth denoising of any non-stationary and nonlinear data. This algorithm can only decompose signals based on its own time scale characteristics, and has a high signal-to-noise ratio, which has great advantages over general denoising methods [15].

The decomposed data of EMD filtering algorithm has extremum and can determine the local time-domain characteristics of the data based on the time scale displacement between the extremum points. Therefore, it is theoretically applicable to the decomposition of any type of time series (signal). The EMD filtering algorithm decomposes complex signals into multiple Intrinsic Mode Functions (IMFs) [16]. The precise implementation goes like this: first, establish the function of the original signal. Next, compute the maximum and minimum value points

above. If the function of the original signal is  $f(x)$ , calculate all the maximum points on the original signal  $f(x)$ , perform three times of spline function fitting to obtain the envelope function  $e_+(x)$  of the maximum value, use the same method to find all the minimum points on the function  $f(x)$  of the original data, and then perform multiple spline function fitting to obtain the envelope function  $e_-(x)$  of the minimum value. The mean of these two envelope lines is regarded as the envelope function  $m_1(x)$  of the mean envelope of the original signal. Finally, use Equation (4) to determine the mean value of the envelope function.

$$m_1(x) = \frac{e_+(x) - e_-(x)}{2} \quad (4)$$

In Equation (4),  $f(x)$  denotes the original signal function,  $e_+(x)$  denotes the maximum value of the envelope function,  $e_-(x)$  denotes the minimum value of the envelope function, and  $m_1(x)$  denotes the mean value envelope function of the original signal. The new signal function is obtained by subtracting the mean baulk function from the original signal function as in Equation (5).

$$h_1^l(x) = f(x) - m_1(x) \quad (5)$$

In Equation (5),  $h_1^l(x)$  denotes the new signal with low frequencies removed. If  $h_1^l(x)$  is not smooth and does not satisfy the two conditions of the definition of the eigenmode function, iterations need to be performed repeatedly until  $h_1^l(x)$  satisfies the definition of the eigenmode function, and the first-order IMF component of the original signal  $f(x)$  is calculated as in Equation (6).

$$imf_1(x) = h_1^k(x) \quad (6)$$

In Equation (6),  $imf_1(x)$  represents the first-order IMF component. The original function is then subtracted from the component functions to obtain a completely new signal function as in Equation (7).

$$r_1(x) = f(x) - imf_1(x) \quad (7)$$

In Equation (7),  $r_1(x)$  denotes the latest function with high frequencies removed. Repeat the above operation to obtain the  $n$ th order IMF component function  $imf_n(x)$ , or to obtain the component  $r_n(x)$ . until what is obtained is a monotonic function or a constant position. Finally, the original signal is decomposed by EMD as in Equation (8).

$$f(x) = \sum_{i=1}^n imf_i(x) - r_n(x) \quad (8)$$

In Equation (8),  $r_n(x)$  is the trend term, and the function  $imf_1(x)$  is the eigenmode function obtained after several EMD decompositions of the original data function. This decomposition process is called "screening process".

### 2.2. Study on RS recognition of time-series spatial distributions combining quadratic difference method and decision tree

Depending on the season, RS recognizes that the vegetation in a particular area can be reflected by the peak frequency value of NDVITSC. Since NDVITSC is a discrete point and not a continuous function, the number of maxima cannot be obtained by derivation, therefore, the study used the discrete point maxima method and the quadratic difference method, which is a simpler algorithm to operate. Among them, the quadratic difference method has been applied several times in the study of the change of vegetation and replanting index [17]. Firstly, using the discrete point maxima method, it is assumed that a pixel is a series  $P$  consisting of discrete points of  $N$  elements as in equation (9).

$$P1 = INTER(P) = P_{i-1} - P_{i+1}. \quad (9)$$

In Equation (9), the point series  $P1$  is the difference between the values of the two elements before and after series  $P$ , and  $INTER$  indicates the function of the two elements before and after making a difference.  $P_{i-1}$  represents the value of the element before  $P$ , and  $P_{i+1}$  represents the value of the element after  $P$ . Determine the positive and negative of each element value, as in Equation (10).

$$P2 = JUDGE(P1) = \begin{cases} -1, P1 < 0 \\ 1, P1 \geq 0 \end{cases}. \quad (10)$$

In Equation (10),  $JUDGE$  denotes the function that determines the positive or negative value of an element. If it is greater than or equal to 0, it is assigned the value of 1, which constitutes the point series function  $P2$ . If the value is less than 0, the image element is assigned the value of -1. Differential value is made to the series  $P2$  to obtain  $P3$  as in Equation (11).

$$P3 = INTER(P2). \quad (11)$$

Finally, the extreme values, i.e., the elements of the series  $P3$  with a value of -2, is calculated as in Equation (12).

$$number = count(P3 = -2). \quad (12)$$

In Equation (12),  $count$  denotes the count function. The research selected quadratic difference algorithm to extract the number of wave crests, most of the previous use of quadratic difference algorithm to extract the number of wave crests is to write the appropriate procedures to achieve, but this research did not carry out the preparation of the procedure, but in the GIS software platform for modelling implementation. From this, the spatial distribution map of vegetation replanting index is obtained through the rule of two-difference operation, and the specific process is shown in Fig. 2.

Perform a differential operation on the filtered NDVI sequence. If the result is greater than or equal to 1, assign it a value of 1. If the result is less than 1, assign it a value

of 0; Next, perform a second difference operation to calculate the frequency of -2 in each NDVI sequence of pixels, and obtain the relevant index distribution of vegetation in the region.

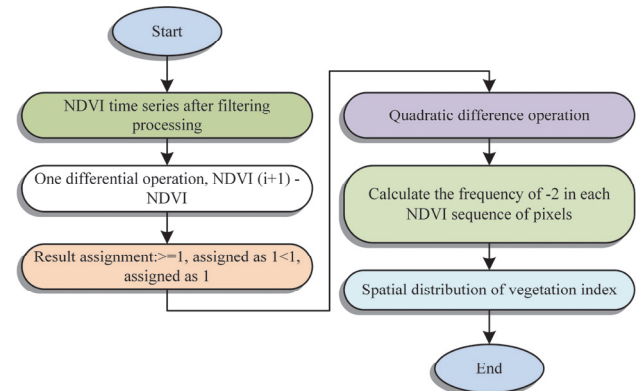


Fig. 2. Flow chart for extracting crop index

In GIS software, the assigned NDVI image data is inputted in chronological order, and the grid subtraction operation is performed by subtracting the previous data from the later data. This will result in a quadratic difference NDVI image data, with only -2, 0, and 2 types of image values after the operation. After FAs filtering, the time series was processed by the quadratic difference method, for example, the occurrence of values -2, 0, 2, -2 indicates the extreme values of the time series, which is able to derive the vegetation situation [18]. The number of changes in an area in a year is the frequency of the peak of the time series NDVI. The frequency of great values in the second difference method is shown in Fig. 3.

In the process of RS identification for gradual optimization, the identification of distinctly different landforms is carried out first. Influenced by the different weather conditions of the climate, the presentation of regional change characteristics in time is not completely consistent, so the annual changes in geographic changes are counted as a range of cycles [19].

The feature extraction process of a decision tree is as follows: First, feature selection is performed, which selects the most valuable features to improve the performance of the decision tree model. Measure through indicators such as information gain and mutual information. Information gain is an indicator of the quality of features, reflecting the degree to which features can reduce entropy (uncertainty). The information gain formula is shown in equation (13).

$$IG(S, A) = H(S) - H(S | A). \quad (13)$$

In Equation (13),  $S$  is the sample set,  $A$  is the feature,  $H(S)$  is the entropy of the sample set, and  $H(S | A)$  is the conditional entropy. Next is feature extraction, which generates new features from the original data to improve the performance of the decision tree model. Extract main directional information from multiple related features.

Afterwards, a decision tree is constructed, which includes selecting the best features, dividing nodes and recursively expanding child nodes.

By constructing a decision tree, assessing the project's risk, and determining the viability of its decision-making analysis method, one can use the decision tree method to determine the probability that the expected value of the net present value is greater than zero. This allows for the reasonable setting of key critical points in decision-making, which in turn allows for the classification of the NDVI time series and the classification of geographical changes in the key period. Vegetation, waters, towns, and forests in a year provide the basis for extracting the feature cover using the decision tree method, and analyzing the four feature covers has the following characteristics, as shown in Table 1.

The forest NDVI feature time-series curve is a single-peaked curve, so the number of peaks is judged first, using a peak of 1 or 2 as a criterion for the first level of sub-nodes. Forests have the unique characteristic of T2 feature, which is used to judge the classification results. Waters have a single-peak NDVI TSC, with a wave peak of 1 as a judgment criterion, using the T2 criterion then get the waters classification results, at this time the data excludes the forest and waters category. Towns and cities were categorized by using T2 as a judgment criterion. The NDVI TSC of other vegetation has a double-peak

characteristic that is obviously different from the other three categories, using the number of wave peaks as a judgment criterion, and finally applying whether the 2nd wave peak is at the time series point to obtain the results of other vegetation, and constructing a decision tree accordingly, as shown in Fig. 4.

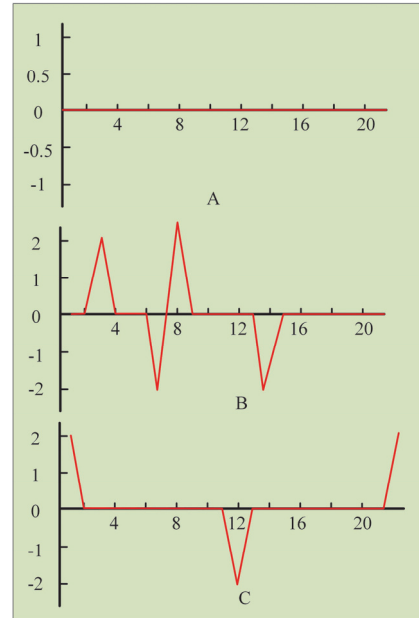


Fig. 3. Maximum frequency in quadratic difference method

Tab. 1. Four types of land cover features

Feature Name	Forest	Waters	Town	Other vegetation
T1	Unimodal	Unimodal	Unimodal	Bimodal
T2	NDVIX 10000 timing points greater than 6000	Less than 500	Timing points are greater than 0 and less than 3000	The first peak appears around timing point 7, and the second peak appears around timing point 14
Case	More than 1/2, less than 2/3	Time series points exceeding 1/2 are less than 0	/	/

A decision tree is a tree like structure in which each leaf node corresponds to a classification, and non leaf nodes correspond to partitions on a certain attribute. Based on the values of the sample on that attribute, it is divided into several subsets. Intermediate data is the data corresponding to each category, used for intermediate classification. Morphological similarity distance (MSD) in the two pairs of multidimensional data metric, can synthesize the object size and shape of the two factors to consider, so the study introduces morphological similarity, the method can be based on the dynamic time bending distance to measure the corresponding time series similarity, and in the algorithm operation has a fast speed, high precision and strong stability in the algorithm operation. Morphological similarity distance can more fully utilize the information provided by NDVI time series data, which is very effective for the accuracy improvement of RS identification [20]. MSD is defined in equation (14).

$$D_{msd} = D_{Euchd} \times \left( 2 - \frac{ASD}{SAD} \right) \quad (14)$$

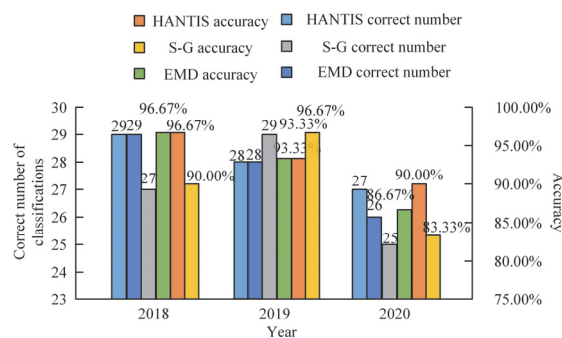


Fig. 4. Constructing a decision tree

In Equation (14),  $D_{Euchd}$  denotes the Euclidean distance between two number series,  $ASD$  denotes the absolute value of the difference of each dimension, and  $SAD$  denotes the Manhattan distance. Let the two multidimensional point data be  $A1 = (x_1, x_2, \dots)$ ,  $A2 = (y_1, y_2, \dots)$ . for the two multidimensional data points  $A1, A2$ , their Euclidean distance as well as Manhattan distance are calculated as in Equation (15).

$$\begin{cases} D_{Euclid} = \sqrt{(x1-y1)^2 + (x2-y2)^2 + \dots} \\ SAD = \sum_{i=1}^n |x_i - y_i|. \end{cases} \quad (15)$$

$A1$ ,  $ASD$  of  $A2$ , denotes the absolute value of the sum of the dimensional values, calculated as in Equation (16).

$$ASD = \left| \sum_{i=1}^n (x_i - y_i) \right|. \quad (16)$$

EMD was used to obtain time-series NDVI data, calculate the morphological similarity distances between points, and qualitatively and quantitatively assess the spatial distribution of RS identification based on the selected thresholds. The MSD method calculates the similarity value between unknown pixels and standard pixels. By selecting an appropriate threshold, the required information can be highlighted and presented intuitively, facilitating the overall understanding and analysis of the spatial distribution of crop patterns and evaluating spatio-temporal changes. To calculate the extraction error of the research area, the formula is shown in equation (17).

$$W = (S - T) / T. \quad (17)$$

In Equation (17),  $S$  represents statistical area,  $T$  represents planting area, and  $W$  represents relative error.

### 3. Experimental verification of RS recognition for FAs reconstructed TSCs

In order to validate the research-proposed RS identification model based on FAs reconstruction TSC, an experiment is hereby carried out to validate it, analyze the corresponding study area parameters and RS data results, verify the advantages and feasibility of the method, and provide a reference for the management of natural resources such as vegetation.

#### 3.1. Experimental data preparation and design

The experiment selected three districts in the plain area of a province as the study area, with an average elevation of about 30 m, an area of 6941 km<sup>2</sup>, and an average annual temperature of 18°C, with 24°C or more lasting for 240 days. The RS data for the experiment comprised data products with a temporal resolution of 18 days and a spatial resolution of 300 m spanning a total of 11 years, from 2013 to 2023. The software used in the study to process the NDVI time series of RS data was ENVI/IDL version 5.4 (The Environment for Visualizing Images/ Interactive Data Language), which has powerful RSI processing capabilities, is suitable for analyzing and processing NDVI series over long periods of time, and is capable of batch processing of the RS data. With narrower red and near-infrared bands, the MODIS sensor is more sensitive to the calculated NDVI to changes in geographic features. The ArcGIS software handles the map information data, and the powerful nu-

merical processing of the Matlab 2016a software is able to be able to handle the time series analysis.

#### 3.2. Measurement statistics and analysis of experimental results

The NDVI time-series profile of one pixel was selected as an example for the experiment, and the NDVI time-series data were processed by HANTS algorithm, S-G algorithm, and EMD filtering, as shown in Fig. 5 for the processing results. It can be seen that the three FAs show large reconstruction differences in the investigation cycle. EMD and S-G filtering reconstruct the profiles similarly, but present greater differences compared with HANTS filtering. S-GFA is too sensitive to noise, and the reconstructed curves show greater differences relative to EMDFA and HANTFA. The HANTS filtered curves, whose baggage lines all include the maxima of the original data, are more effective in dealing with outliers, while the EMD filtered curves do not handle outliers as well as the HANTSFA.

Root Mean Squared Error (RMSE) is an indicator used to measure the prediction accuracy of a prediction model on continuous data. It measures the root mean square difference between predicted and true values, representing the average degree of deviation between predicted and true values. The experiment evaluates the mean square error of the approximate quality of the selected filter time series, as shown in Fig. 6. It can be seen that the RMSE of the EMD-FA proposed in the study is less than 0.1, while the traditional method is stable at around 0.15, indicating that the filtering effect of the algorithm proposed in the study is better.

The peaks and valleys of the NDVI of vegetation with a one-year growth cycle and a six-month growth cycle are depicted in Fig. 7, together with the red dashed line designating the peak scenario. The NDVI curves are the curves that can most intuitively reflect the process of changes in vegetation NDVI, and analyze the replanting index of vegetation through the NDVI index. Fig. 7a illustrates that the NDVI of vegetation with one year as the growth cycle forms a single-peaked NDVITSC during the year, and Fig. 7b illustrates that the NDVI of vegetation with half a year as the growth cycle forms a double-peaked NDVITSC during the year.

Fig. 8 illustrates typical vegetation NDVI time-series curves, indicating a clearer separation of spring and fall seasons when the annual cumulative day reaches approximately 150. Consequently, the boundary for vegetation NDVI time-series curve segmentation can be set at a cumulative day of 150, allowing for the acquisition of typical spring and fall vegetation NDVI time-series curves. The late June to mid-August, early March to mid-April, and early June to mid-August are when the NDVI values peaked.

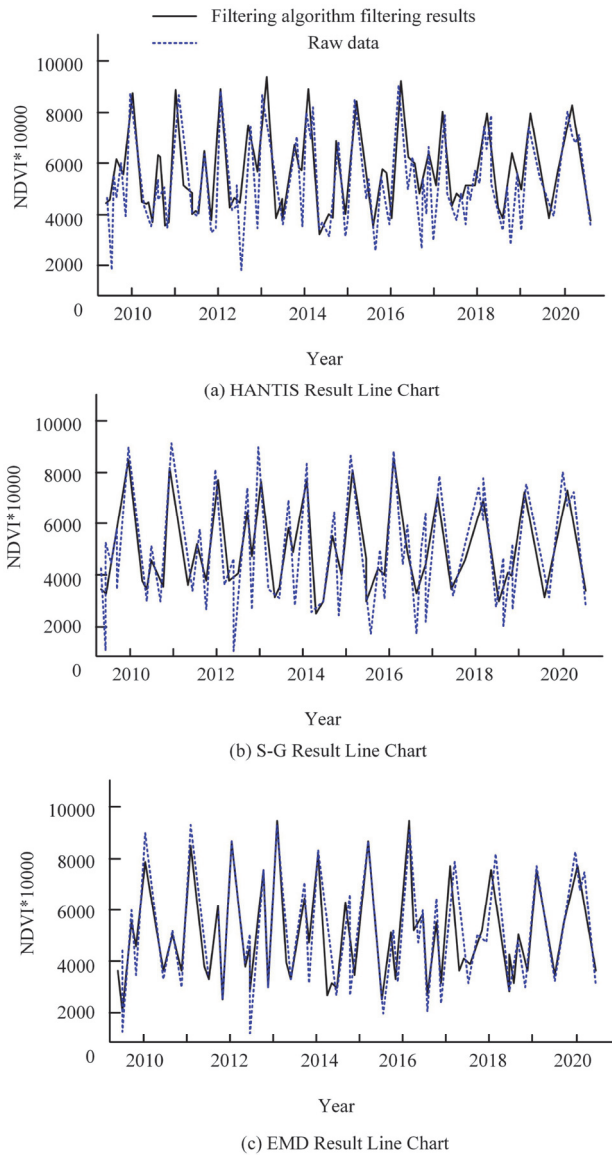


Fig. 5. The results of processing NDVI time series data from 2010 to 2020 using HANTS algorithm, S-G algorithm, and EMD filtering

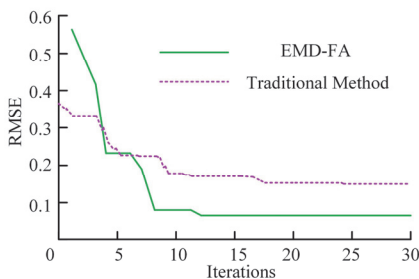


Fig. 6. Evaluation of the mean square error of the selected filter time series approximation quality

Fig. 9 shows the error analysis of the study area extraction of the three algorithms. With the selection of different filtering and denoising algorithms, the results of the quadratic differential identification of vegetation conditions varied, but by comparing the recurrence indices calculated by the three FA, the relative errors of the three

FAs were less than 10%, only S-GFA had a recurrence index of more than 2 in the 2014 data, and the recurrence indices of the other years of the HANTSFA, the EMDFA, and the S-GFA were all less than or close to 2.

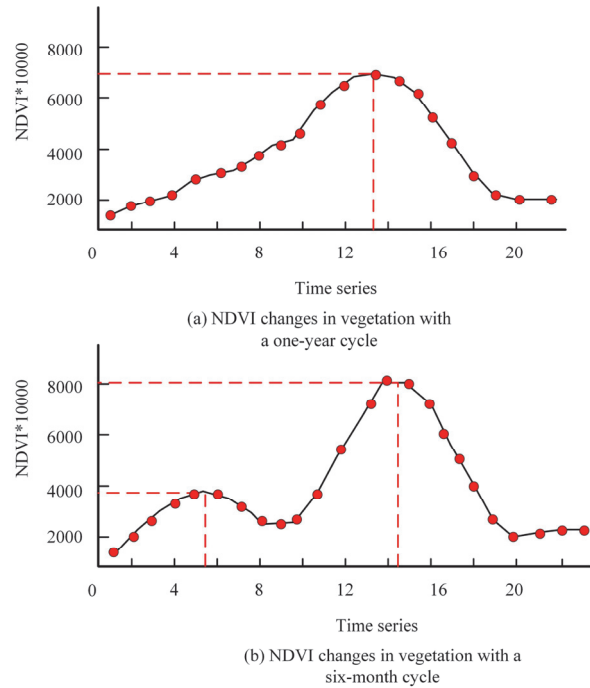


Fig. 7. NDVI time series change curve of vegetation

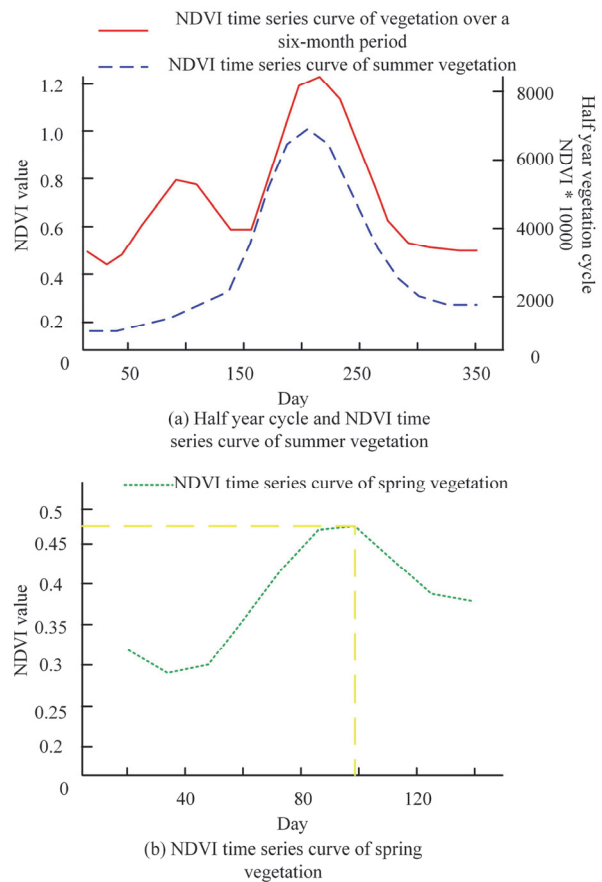


Fig. 8. Typical NDVI time series curve of vegetation

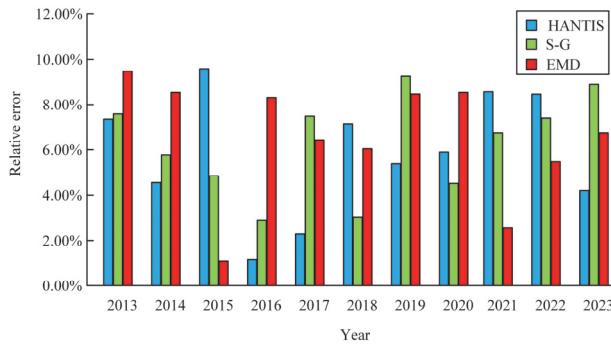


Fig. 9. analysis of error in extracting the area of the study area

For the extraction of NDVI TSC of feature characteristics, the study is based on manually selecting feature points, so as to extract the characteristic curves of towns, waters, and forests, as shown in Fig. 10. The watershed and town are more gentle, the forest TSC is steeper, and the three are obviously characterized by a single peak. In one year, the NDVI of towns is larger than that of waters, and the NDVI of waters is basically near and below the value of 0. The NDVI of forests is larger than that of waters and towns, and although the waveforms of the three are similar, the differences are high. The analysis shows that the forest NDVI curve has obvious single-peak characteristics and lasts for a longer period of time. NDVI, as a kind of vegetation monitoring index, is less sensitive to waters and towns because of their lower vegetation coverage, while the fluctuation and undulation of NDVI in waters and towns are significant.

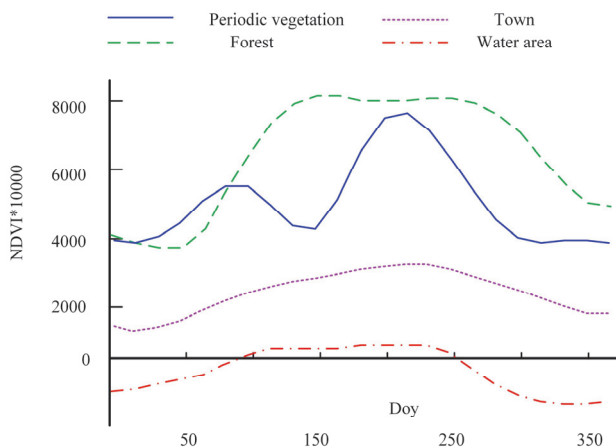


Fig. 10. NDVI time series curve of forest, water area, and town

The area of the study area following the year corresponding to each FA in the figure was extracted by Matlab in order to further quantify the results of spatial distribution. Statistical analysis of the data was used to determine the correct number and accuracy of the vegetation identification classification for each year in Fig. 11. In Fig. 11, the accuracy of the ground validation points based on the decision tree method under the three FAs is above 80%, which has high accuracy, among which the average value of the accuracy in 2019 reaches 96.67%,

which is the highest accuracy among the statistical years, so the FAs of this study have the advantage of accuracy.

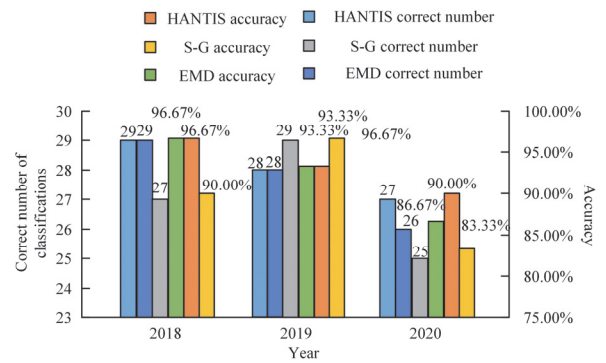


Fig. 11. The positive number and accuracy of vegetation recognition classification for each filtering method corresponding to the year

During the investigation of the ground verification points, the investigators selected the land with a planting area of more than 10 mu, and the auxiliary tool of the ground verification points was the GPS handheld of Trimble Company to collect the geographical and spatial coordinates on the spot. Select a total of 30 ground verification points in the three areas of the plain. After completing the ground survey points, return to the laboratory and compare the planting patterns of these 30 ground validation points on the map through Google Earth. Based on the morphological similarity method, the spring and fall vegetation distribution maps can be obtained, and the accuracy validation results are shown in Table 2. There are a total of 30 ground validation points selected in the field, and the study takes each year as a time interval and selects ground validation points year by year, and the land types that can be recognized are different, for the fall plants, the mapping accuracy is the highest in 2013, 97.37%, and the mapping accuracy is the lowest in 2014, 80.00%. For spring plants, 2017 had the greatest mapping accuracy at 97.96%, and 2014 had the lowest, but again more favorable, mapping accuracy at 90.00%.

4. Conclusion

To suppress noise during RSI processing, the image must be filtered. The traditional FAs technique is ineffective in noise processing of vegetation image RS. Hence, the study recommends using FAs to reconstruct TSC of vegetation for improved recognition while acknowledging noise. Additionally, combining the quadratic difference method, decision tree, and MSD enhances recognition ability and RSI accuracy. Experiments were conducted to validate the proposed method. The results indicated an average accuracy of 96.67% in 2019, the highest among the statistical years. When considering each year as a time interval and for fall plants, the highest mapping accuracy of 97.37% was achieved in 2013, and the lowest mapping accuracy of 80.00% was achieved in 2014. For the spring crops, the highest level of accuracy in mapping, at 97.96%, was attained in 2017, while the least accuracy in mapping,

90.00%, was attained in 2014. When assessing the replanting indices calculated by all three FA, just the S-GFA had a replanting index exceeding 2 in the 2014 data. On the other hand, the replanting indices of the HANTSFAEMDFA and the S-GFA were either less than or almost 2 for the other years. Furthermore, the relative errors of all three FAs were less than 10%. The ground validation points have accuracies above 80% based on the decision tree method, revealing the superiority of the FAs in this study with respect to accuracy. While the proposed method displays good accuracy and vegetation recognition

ability, it is impacted by the resolution of the initial image, the estimation of area, and the intricacy of validation procedures. Although the methods proposed in the study have good vegetation recognition capabilities and accuracy, there are still certain shortcomings in the research due to the resolution, area estimation, and verification complexity of the original images. For example, insufficient consideration was given to remote sensing situations of images with different resolutions, and the setting of ground verification points was not sufficient. Improvement and accuracy improvement are needed in future research.

Tab. 2. Accuracy verification results of spring and autumn vegetation distribution map based on morphological similarity method

Year		2013	2014	2015	2016	2017	2018	2019	2020	2021	2022	2023
Map- ping ac- curacy	Reference points	38	20	22	24	49	25	36	33	25	38	45
	Correct classification number	37	18	20	23	48	23	35	32	24	34	42
	Spring classification accuracy, %	97.37	90.00	90.91	95.83	97.96	92.00	97.22	96.97	96.13	90.21	93.08
	Correct classification number	37	16	19	21	44	22	34	31	22	33	41
	Autumn classification accuracy, %	97.37	80.00	86.36	87.50	89.80	88.00	94.44	93.94	94.16	85.29	87.95

**References**

[1] Ahmad M, Shao Z, Altan O. Effect of locust invasion and mitigation using remote sensing techniques: a case study of North Sindh Pakistan. *Photogramm Eng Rem S* 2022; 88(1): 47-53. DOI: 10.14358/PERS.21-00025R2.

[2] Deng X, Tang G, Wang Q. A novel FAT classification filtering algorithm for LiDAR point clouds based on small grid density clustering. *Geod Geodyn* 2022; 13(1): 38-49. DOI: 10.1016/j.geog.2021.10.002.

[3] Sun C, Li J, Liu Y, et al. Plant species classification in salt marshes using phenological parameters derived from Sentinel-2 pixel-differential time-series. *Remote Sens Environ* 2021; 256: 112320. DOI: 10.1016/j.rse.2021.112320.

[4] Bao R, Zhang J, Lu C, et al. Estimating above-ground biomass of *Pinus densata* Mast. Using best slope temporal segmentation and Landsat time series. *J Appl Remote Sens* 2021; 15(2): 024507. DOI: 10.1117/1.JRS.15.024507.

[5] Liu R, Huang F, Ren Y, et al. Characterizing ecosystem functional type patterns based on subtractive fuzzy cluster means using Sentinel-2 time-series data. *J Appl Remote Sens* 2020; 14(4): 48505. DOI: 10.1117/1.JRS.14.048505.

[6] Lian X, Liu X, Ge L, et al. Time-series unmanned aerial vehicle photogrammetry monitoring method without ground control points to measure mining subsidence. *J Appl Remote Sens* 2021; 15(2): 024505. DOI: 10.1117/1.JRS.15.024505.

[7] Fan Y, Zhao C, Yu H, et al. Dynamic load identification algorithm based on Newmark-β and self-filtering. *P I Mech Eng C-J Mec* 2020; 234(1): 96-107. DOI: 10.1177/0954406219869981.

[8] Yang T, Yu H, Wang Y. An efficient low-pass-filtering algorithm to de-noise global GRACE data. *Remote Sens Environ* 2022; 283: 113303. DOI: 10.1016/j.rse.2022.113303.

[9] Rayegani B. Sand and dust storm sources identification: A remote sensing approach. *Ecol Indic* 2020; 112(May): 106099. DOI: 10.1016/j.ecolind.2020.106099.

[10] Wang Z, Tian S. Ground object information extraction from hyperspectral remote sensing images using deep learning algorithm. *Microprocess Microsy* 2021; 87(Nov): 104394. DOI: 10.1016/j.micpro.2021.104394.

[11] Dharejo FA, Zhou Y, Deeba F, et al. A remote-sensing image enhancement algorithm based on patch-wise dark channel prior and histogram equalisation with colour correction. *IET Image Process* 2020; 15(3): 47-56. DOI: 10.1049/ipr2.12004.

[12] Gong M. Multimedia digital signal processing of infrared chemical remote sensing based on piecewise linear discriminant algorithm. *Adv Multimed* 2021; 2021(Pt 1): 6337431. DOI: 10.1155/2021/6337431.

[13] Li S, Dai Z, Cai M. A novel DVAPSO-LSTSVM classifier in compressed sensing domain for intelligent pipeline leakage diagnosis. *Process Saf Environ* 2023; 175: 447-460. DOI: 10.1016/j.psep.2023.05.065.

[14] Aliyan SA, Bahri AS, Widodo A, et al. Remote sensing data integration of landsat 8 and SRTM for geomorphological characteristics identification in. *Int J Adv Sci Eng Inform Technol* 2020; 10: 212-218. DOI: 10.18517/ijaseit.10.1.6751.

[15] Khan B, Rathore VS, Krishna AP. Identification of desakota region and urban growth analysis in Patna City, India using remote sensing data and GIS. *J Indian Soc Remote Sens* 2021; 49(4): 935-945. DOI: 10.1007/s12524-020-01248-8.

[16] Wu S, Wang J, Yan Z, et al. Monitoring tree-crown scale autumn leaf phenology in a temperate forest with an integration of Planet Scope and drone remote sensing observations. *ISPRS J Photogramm* 2021; 171: 36-48. DOI: 10.1016/j.isprs.2020.10.017.

- [17] Bersi M, Saibi H. Groundwater potential zones identification using geoelectrical sounding and remote sensing in Wadi Touil plain, Northwestern Algeria. *J Afr Earth Sci* 2020; 172: 104014. DOI: 10.1016/j.jafrearsci.2020.104014.
- [18] Ouhoussa L, Ghafiri A, Aissi LB, et al. Integrating aster images processing and fieldwork for identification of hydrothermal alteration zones at the Oumjrane-Boukerzia District, Moroccan Anti-Atlas. *Open J Geol* 2023; 13(2): 171-188. DOI: 10.4236/ojg.2023.132008.
- [19] Masood F, Masood J, Zahir H, et al. Novel approach to evaluate classification algorithms and feature selection filter algorithms using medical data. *J Comput Cog Eng* 2023; 2(1): 57-67. DOI: 10.47852/bonviewJCCE2202238.
- [20] Fang Y, Luo B, Zhao T, et al. ST-SIGMA: Spatio-temporal semantics and interaction graph aggregation for multi-agent perception and trajectory forecasting. *CAAI T Intell Techno* 2022; 7(4): 744-757. DOI: 10.1049/cit2.12145.

---

#### *Authors' information*

**Mengxue Li** obtained her master's degree in Engineering (2017) from North China University of Water Resources and Electric Power. She is working as a lecturer and a full-time teacher at Zhengzhou University of Science and Technology. She was invited as a resource person to deliver various technical talks on artificial intelligence, pattern recognition, and algorithm design. She also served as the vice dean of teaching of Zhengzhou Information Engineering Vocational College, and managed the teaching and research work of the department. She has published more than 10 papers on scientific research and teaching research in well-known domestic journals. Her areas of interest include artificial intelligence, machine learning, pattern recognition, and image processing. E-mail: [limxue2023@163.com](mailto:limxue2023@163.com)

**Chenjian Xu** obtained a master's degree from Yunnan Normal University. He has previously worked as a Network and Security Technology Engineer at China Mobile Communications Corporation (CMCC), and currently serves as the Director of the Information Center at Zhengzhou Information Engineering Vocational College, engaged in education informatization related work. I have conducted in-depth research on artificial intelligence technology and information security technology, and have presented several related research results. E-mail: [ly0446@hati.edu.cn](mailto:ly0446@hati.edu.cn)

---

*Received January 24, 2024. The final version – June 18, 2024.*

---